

HACK: Homomorphic Acceleration via Compression of the Key-Value Cache for Disaggregated LLM Inference

Zeyu Zhang
University of Virginia

Haiying Shen
University of Virginia

Shay Vargaftik
VMware Research

Ran Ben Basat
University College London

Michael Mitzenmacher
Harvard University

Minlan Yu
Harvard University

ABSTRACT

Disaggregated Large Language Model (LLM) inference has gained popularity as it separates the computation-intensive prefill stage from the memory-intensive decode stage, avoiding the prefill-decode interference and improving resource utilization. However, transmitting Key-Value (KV) data between the two stages can be a bottleneck, especially for long prompts. Additionally, the computation time overhead for prefill and decode is key for optimizing Job Completion Time (JCT), and KV data size can become prohibitive for long prompts and sequences. Existing KV quantization methods can alleviate the transmission bottleneck and reduce memory requirements, but they introduce significant dequantization overhead, exacerbating the computation time.

We propose Homomorphic Acceleration via Compression of the KV cache (HACK) for disaggregated LLM inference. HACK eliminates the heavy KV dequantization step, and directly performs computations on quantized KV data to approximate and reduce the cost of the expensive matrix-multiplication step. Extensive trace-driven experiments show that HACK reduces JCT by up to 70.9% compared to disaggregated LLM inference baseline and by up to 52.3% compared to state-of-the-art KV quantization methods.

1 INTRODUCTION

LLM inference is the process of generating answers to incoming requests (prompts), and its optimization is crucial for reducing costs, enhancing scalability, lowering energy consumption, and enabling deployment on commodity GPUs. LLM inference has two stages: prefill and decode. The prefill stage processes the prompt, incurring significant compute overhead that scales with both prompt length and model size. The decode stage generates one token at a time per prompt and is memory-intensive, since it must store Key-Value (KV) data that expands with the sequence length.

Traditionally, prefill and decode run on the same GPU, causing interference: the prefill stage’s compute load delays the decode stage, whereas the decode’s memory footprint reduces the supported number of concurrent prefill operations.

Although high-end GPUs offer sufficient memory and computational power for both stages, their high cost is a limiting factor. Disaggregated LLM inference addresses this issue by splitting the stages between different compute-focused GPUs (e.g., A10G, V100, T4, L4) for prefill, and larger-memory GPUs (e.g., A100, H100) for decode [24, 25, 30, 40–42, 52]. This separation eliminates performance interference and improves overall GPU utilization, making LLM inference more efficient and cost-effective.

The prefill GPU must send its KV data to the decode GPU over the network. However, inexpensive GPU instances from cloud providers often lack high-speed networking. For example, AWS’s A10G, V100, T4, and L4 instances cost roughly 10–20 times less than A100 instances—which typically offer 400 Gbps bandwidth—but their network speeds are limited to 10–50 Gbps or lower [10]. Similarly, Tencent Cloud’s A100 instances are configured with only 5–50 Gbps bandwidth to cut costs [14]. As a result, KV transmission between the prefill and decode instances can become a bottleneck, impairing end-to-end performance. Our measurements (§2) show that this overhead can account for up to 42.2% of Job Completion Time (JCT). With the growing popularity of KV data sharing across requests [36, 41] to reduce computation time in disaggregated LLM inference, the communication bottleneck is expected to worsen.

Pipelining communication to overlap with prefill computation [40] can reduce communication overhead. However, if communication time greatly exceeds prefill time, this approach loses effectiveness. Additionally, when the prefill instance lacks sufficient GPU memory across decode instances to store decode-specific data, it must temporarily transfer KV data to CPU memory [42], rendering pipelining infeasible.

Computation can also become a bottleneck; in our measurements (§2), prefill and decode times account for up to 45.6% and 83.3% of JCT, respectively. Moreover, during the decode stage, GPU memory is constrained by the large volume of cached KV data [40, 52]. Memory usage can reach up to 93.7%. Memory access latency for KV data can consume up to 33.1% of JCT.

These issues become more pronounced in long-prompt and long-sequence applications, such as book summarization,

	Reducing KV communication	Reducing compute	Reducing memory access latency for KV	Avoiding KV dequantization	Achieving high KV compression rate
Baseline	×	×	×	✓	×
KV quantization	✓	×	✓	×	✓
FP4/6/8	✓	Require hardware	✓	Require hardware	×
HACK	✓	✓	✓	✓	✓

Table 1: Features of different methods and our system HACK.

article writing, and coding, which have surged in popularity. In fact, commercial models like Gemini 1.5 [21] now support a context window of up to 1M.

KV quantization methods, such as CacheGen [36] and KVQuant [23], can alleviate the transmission bottleneck and reduce memory access latency during decoding. These approaches quantize the KV data after each iteration before storing it in the cache, then retrieve and dequantize all tokens’ KV data in the next decode iteration. However, they introduce significant KV dequantization overhead. When we employ CacheGen and KVQuant in the disaggregated LLM inference, the dequantization overhead can account for up to 37.9% of JCT (§2).

Lower precision Floating Point (FP) formats (e.g., FP4 [45], FP6 [47], and FP8 [44]) can reduce KV size and accelerate computation when supported by hardware. They provide up to 73% KV compression [8], compared to the 86% [23, 36] achieved by CacheGen and KVQuant through mixed-precision and 2-bit quantization. However, for FP4 and FP6, current GPUs require conversion to FP8 or FP16 for computation. On GPUs without FP8 support—such as pre-H100 architectures like the A100—FP8 must be converted to FP16, introducing additional computational overhead.

Ideally, arithmetic operations should be executable directly on quantized KV data, eliminating dequantization overhead and accelerating computation through smaller data elements. To this end, we propose Homomorphic Acceleration via Compression of the KV cache (HACK) for disaggregated LLM inference. HACK addresses the KV transmission bottleneck by enabling computation on quantized data while maintaining comparable inference accuracy and reducing memory constraints. Table 1 summarizes the advantages of HACK over earlier approaches.

In summary, our work has the following contributions:

- We propose a homomorphic quantization method for matrix multiplication. It conducts KV-related matrix multiplication on quantized matrices without the need for dequantizing them and then applies an approximation to transform the quantized output into an approximation of the real output. This approach reduces KV transmission latency, computation time, memory access latency, and memory demand, all while avoiding the costly overhead of KV dequantization.

- We further reduce the overhead of homomorphic quantization by storing data using a small amount of memory to eliminate redundant computations and the need to update the quantized data.
- We integrate HACK into FlashAttention-2 [18] and build our system on vLLM [32]. We conduct extensive experiments across various models, datasets, and GPU configurations. These experiments demonstrate that HACK can reduce JCT by up to 70.9% and 52.3% compared to the disaggregated LLM inference baseline and state-of-the-art KV quantization methods, respectively. We open-sourced the code of HACK [2].

2 MOTIVATION

We investigate the networking, computation, and memory bottlenecks in disaggregated LLM inference and demonstrate the limitations of current KV quantization methods in addressing these issues. The default experiment settings are detailed in §7.1.

2.1 Bottlenecks in Disaggregated LLM Inference

The popularity of disaggregation has led to the adoption of cheaper GPU instances for prefill to reduce costs [24, 25, 30, 40–42, 52]. However, this also exacerbates certain overheads. **Network and computation overhead.** To demonstrate the network and computation overhead when using varying prefill instances, we tested Llama-3.1 using the Cocktail on A100, T4, A10G, L4, and V100. Fig. 1(a) shows the average prefill time ratio, average communication time ratio, and average decode time ratio. The average time ratio is calculated by $\frac{1}{N} \sum_{i=1}^N (\frac{\text{time}_i}{\text{JCT}_i})$, where time_i and JCT_i denote the time and JCT of request i , respectively. A100, equipped with a 400 Gbps network, achieves a 3.7% average communication time ratio, while other instances with 10–50 Gbps networks range from 19.1–23.5%. The average prefill time ratio and the average decode time ratio are 19.7%–41.4% and 43.1%–82.5%, respectively.

Next, we tested the performance of different models using the Cocktail dataset. Since Falcon-180B has a limitation of 2K context window, it cannot process Cocktail. Therefore, we used another long-sequence dataset, arXiv [15], for Falcon

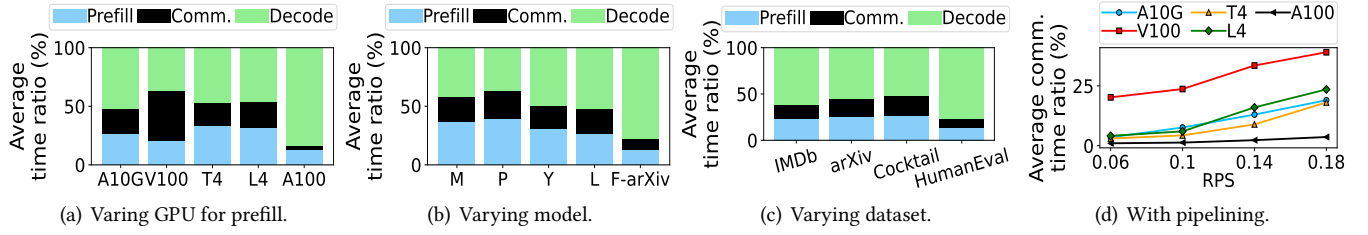


Figure 1: Bottlenecks in disaggregated LLM inference.

180B, and denote it as F-arXiv. Fig. 1(b) shows the average time ratios. The average communication time ratio is 11.8% for F-arXiv and 18.7%-25.3% for other models. The average prefill time ratio and the average decode time ratio are 17.6%-45.6% and 39.8%-81.7%, respectively.

Fig. 1(c) presents the average time ratios for Llama-3.1 70B across various datasets on A10G prefill instances. The average communication time ratio, driven by input sequence length, varies from 9.5% to 21.9%. The average prefill and decode time ratios are 13.6%-37.1% and 54.8%-83.3%, respectively. The arXiv and Cocktail datasets, with long prompts and sequences, incur 15.5-43.1× higher KV communication time and 9.8-19.2× higher computation time compared to the shorter IMDb and HumanEval datasets.

Memory overhead. To illustrate the memory bottleneck, we measured peak GPU memory usage on decode instances for Llama-3.1 70B across different datasets. This metric represents the ratio of memory required for parameters, KV data, and activations to the total memory capacity, ranging from 65.3% to 93.7% (Table 5). We also measured GPU memory access time for loading KV data during decode, with an average ratio of 16.3%-33.1%.

OBSERVATION 1. *In disaggregated LLM inference, KV transmission can contribute up to 42.2% of JCT, with prefill and decode times reaching 45.6% and 83.3%, GPU memory usage up to 93.7%, and KV memory access up to 33.1%, creating significant bottlenecks.*

Pipelining for reducing communication overhead. As indicated in §1, pipelining i) cannot mitigate communication overhead when communication time significantly exceeds prefill time, and ii) is infeasible when GPU memory is insufficient on all decode instances. In case ii), the prefill instance transfers the KV data to its CPU memory [42]. We tested Llama-3.1 with Cocktail on various prefill instances with pipelining. Fig. 1(d) shows the average communication time ratio with different requests-per-second (RPS). When RPS increases from 0.06 to 0.18, the average communication time ratio on V100 rises from 21.4% to 39.2%, which reflects case i) above. For A10G, T4, and L4, this ratio increases from 3.3%-4.1% to 18.7%-23.5%, which reflects case ii) above. When RPS

is 0.18, the decode instances have insufficient GPU memory. On A100 with high bandwidth, this ratio grows from 1.4% to 3.7%. The results demonstrate the limitations of pipelining; it is primarily suitable for scenarios with low KV transmission overhead and light workloads. In this paper, we focus on reducing KV communication overhead through quantization, as opposed to relying on pipelining.

2.2 Overhead for KV Quantization

Quantization methods can be used to reduce the KV transmission overhead and the memory overhead during decode. However, they must dequantize all tokens’ KV values retrieved from the KV cache before computation in every decode iteration, which incurs substantial dequantization overhead. CacheGen [36] and KVQuant [23] are representative of the state-of-the-art. CacheGen focuses on leveraging KV data’s distributional properties to encode it into more compact bitstream representations. KVQuant, on the other hand, targets low-precision KV quantization with 2-bit precision. Both can achieve up to approximately 86% KV compression rates with approximately 98% of baseline accuracy.

As strawman methods, we implemented CacheGen and KVQuant in the baseline disaggregated LLM inference. On the prefill instance, the methods quantize KV data using CacheGen or KVQuant and transmit the quantized KV data to the decode instance, which dequantizes the data back to FP16 before conducting the attention computation.

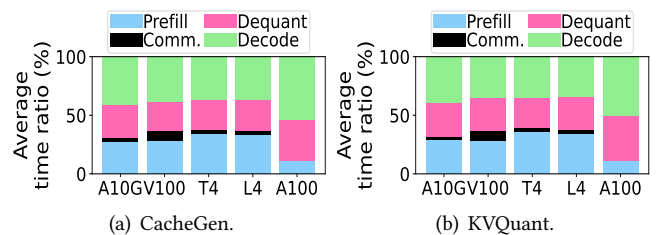


Figure 2: Employing KV quantization across prefill instances.

Fig. 2, 3, and 4 illustrate the average prefill time ratio, communication time ratio, dequantization time ratio, and decode time ratio with different prefill instances, models, and datasets, respectively. Comparing Fig. 2 with Fig. 1(a),

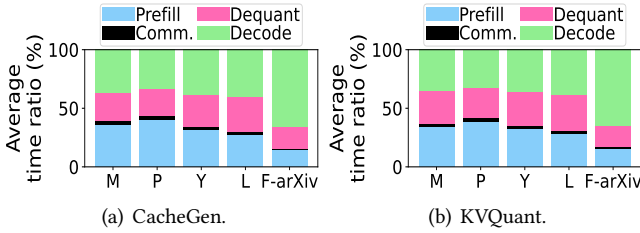


Figure 3: Employing KV quantization across models.

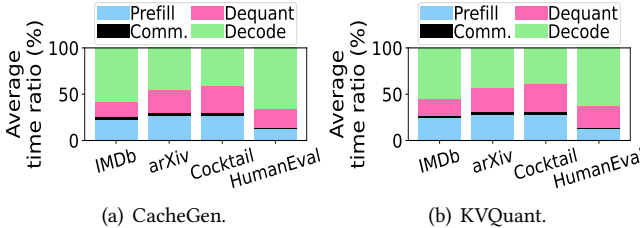


Figure 4: Employing KV quantization across datasets.

we observe that for the A100, T4, A10G, L4, and V100 prefill instances, CacheGen and KVQuant reduce the average communication time ratio by 3.13%-3.25%, 16.18%-16.39%, 18.5%-18.84%, 19.81%-20.27%, and 33.5% and 34.1%, respectively. However, the average KV dequantization time ratios for other instances range from 26.4% to 37.9%. This demonstrates that the dequantization overhead introduced in each decode iteration negatively impacts the end-to-end performance.

Comparing Fig. 3 and Fig. 1(b), we see that CacheGen and KVQuant reduce the average communication time ratio by 10.26%-21.63%. However, for all models, they have an average dequantization time ratio of 18.2%-30.8%. Comparing Fig. 4 and Fig. 1(c), we see that CacheGen and KVQuant reduce the average communication time ratio by 8.19%-18.73%. However, they have average dequantization time ratios of 17.2%-30.4%. Long-sequence datasets have 12.4-24.9 \times dequantization time compared to short-sequence datasets because more KV data is dequantized.

Our measurement results from Llama-3.1 70B with different datasets indicate that CacheGen and KVQuant reduce the peak memory usage on decode instances by 15.7%-19.6% for short-sequence datasets and by 26.9%-33.6% for long-sequence datasets (Table 5). They reduce the average JCT by 13.6%-24.1% by decreasing memory access time for KV data.

The computation times are the same between the baseline and KV quantization methods because they all perform computation on the original FP16 data.

OBSERVATION 2. *Although KV quantization methods can effectively reduce the KV transmission overhead, memory usage, and KV memory access time in disaggregated LLM inference, they introduce additional KV dequantization overhead up to 37.9% of JCT, which is even higher for long-sequences. Additionally, they cannot reduce computation time.*

3 LOW-PRECISION FLOATING POINTS

Low-precision FP4/6/8 can accelerate computation when hardware supports them. However, NVIDIA GPUs with pre-H100 architectures do not support FP8 computation. FP4/6 needs to be converted to FP8 or FP16 for computation, leading to conversion overhead. Furthermore, FP4/6/8 cannot achieve a high KV compression rate to minimize the communication overhead and KV memory access time.

Since none of the GPUs in the experiments support FP8 computation, we conducted a simulation test to measure the communication overhead and KV memory access time for FP4/6/8 using Llama-3.1 70B, Cocktail and different prefill instances. We converted KV data from FP4/6/8 to FP16 before attention computation, and then manually halved the time spent in matrix multiplication in attention to simulate FP8 computation. The simulation results show that FP4, FP6, and FP8 can have an average KV communication time ratio of up to 24.3%, 32.3%, and 37.5%, respectively. The average KV memory access time ratio is 10.7%-19.4%. These simulation results indicate that FP4/FP6/FP8 cannot effectively minimize the communication and memory access time overhead due to the low KV compression rate.

4 BACKGROUND

LLM inference basics. LLM inference consists of two stages: prefill and decode. During the prefill stage, the model processes a sequence of input tokens, also referred to as the prompt. The LLM processes the input tokens to generate the first token. This first token is then used in the decode stage, where it is fed back into the model to generate the next token. The generated token serves as the input for the next decode iteration, and the process repeats iteratively to generate subsequent tokens. LLMs consist of multiple identical layers and use the attention mechanism [4] in each layer to evaluate the interdependencies between tokens in a sentence across different aspects represented by different attention heads. The input tokens, represented by the embedding matrix E , are transformed into a query matrix Q^h , a key matrix K^h , and a value matrix V^h in each attention head h by:

$$Q^h = EW_Q^h, K^h = EW_K^h, V^h = EW_V^h, \quad (1)$$

where W_Q^h , W_K^h , and W_V^h are the parameter matrices. In prefill, the input tokens' Q^h , K^h , and V^h are used for self-attention

computation, and K^h and V^h are cached in memory for reuse in the decode stage. In decode, the input token’s K^h and V^h are respectively combined with all previous tokens’ K^h and V^h in the cache to form the new K^h and V^h that will be used in the self-attention computation. The self-attention computes the output O^h of head h by:

$$O^h = \text{softmax}\left(\frac{Q^h(K^h)^T}{\sqrt{d_h}}\right)V^h = P^hV^h. \quad (2)$$

The *softmax* function operates row-wise on the input matrix $[x_{i,j}]$ as follows:

$$\frac{\exp(x_{i,j})}{\sum_{k=1}^{t_i} \exp(x_{i,k})}, \quad (3)$$

where t_i is the index of the token on row i . The outputs from all heads are concatenated together along the head dimension to form the self-attention output O . The model further processes O through a linear transformation, a Multi-Layer Perceptron (MLP), and other operations to finally produce logits, which are used to generate an output token. Self-attention accounts for a large proportion of computational overhead in the entire process.

Disaggregated LLM Inference. In disaggregated LLM inference, during the prefill stage, the prompt tokens’ Q , K , and V are generated and used for self-attention on the prefill instance. The prefill stage outputs the first token, which is then transferred to the decode instance along with the KV data of prompt tokens. If no decode instance has enough memory to serve the request, the prefill instance temporarily stores the first token and KV data in its CPU memory until a decode instance is available [42]. On the decode instance, the first token is fed to the model as the input, and its Q , K , and V are generated. The input token’s K and V are combined with the previous tokens’ K and V . The input token’s Q and the combined K and V are used for self-attention computation. The decode iteration outputs the next token, which will be fed into the decode model as the next input, followed by the same steps in the decode stage. This process repeats until the maximum output length is reached or the End-of-Sentence (EOS) token is output.

5 SYSTEM DESIGN

5.1 Overview

Observation 1 implies that we need to reduce the communication time, computation time, and memory access latency for KV. Therefore, we can use quantized KV values. However, this will generate high dequantization time overhead based on Observation 2. To quantize KV values while eliminating the dequantization time overhead, HACK provides homomorphic quantization on KV-related matrix multiplications. Employing HACK in the disaggregated LLM inference reduces the KV data transmission time, the computation time, and the memory access latency for KV, thereby improving

end-to-end response time. Fig. 5 illustrates the workflow of employing HACK in the disaggregated LLM inference. Since CacheGen has a KV compression rate of 86%, and KVQuant uses 2-bit quantization to achieve a similar compression rate, we also use 2-bit quantization for KV. The prefill instance generates Q , K , and V from prompt tokens (①) and quantizes them to Q' , K' , and V' (②). Q will be discarded right after computation, which means the quantized Q' does not need to have a minimal size to save space. Thus, Q uses 8-bit quantization rather than 2-bit to increase accuracy. The first matrix multiplication between Q' and K' as in Eq. (2) is performed using homomorphic quantization (③) to output attention score S without the need to dequantize K' , accelerated by GPU’s INT8 computation capacity. The attention score S is transformed to attention probability P via *softmax* in Eq. (3) (④), which is then quantized to P' using INT8 quantization for accuracy (②). P' and V' are multiplied using homomorphic quantization for acceleration (③). The self-attention output O is processed by further operations to finally output the first token (⑤). If no decode instance has enough GPU memory, the prefill instance will swap the quantized KV data to CPU memory (⑥). When a decode instance has enough memory, the prefill instance transmits the first token, K' , V' , and the quantization metadata, the minimum value m and the scale value s , to the decode instance (⑦). K' and V' are stored in KV cache on the decode instance (⑧). The decode instance generates the Q , K , and V from the first token (①) and quantizes them to Q' , K' , and V' (②) as on the prefill instance. The first token’s K' and V' are merged with all prior tokens’ K' and V' along the token dimension, respectively (⑨). The homomorphic quantization for the first token’s Q' and the updated K' and V' is performed in the same way as prefill. The next token is generated through further operations (⑤) and fed to the model to proceed to the next decode iteration (①).

5.2 Homomorphic Quantization for Matrix Multiplication

KV-related computation in Eq. (2) involves two matrix multiplications: $Q^h(K^h)^T$ and P^hV^h . We aim to perform multiplication on two quantized matrices to leverage the GPU’s INT4 or INT8 computation capabilities without the need to dequantize matrix values before computation to get an approximation of the true output. For this goal, we propose homomorphic quantization for the matrix multiplications. That is, for matrix multiplication $C = AB$, the method first quantizes A and B to obtain A' and B' . It then performs the matrix multiplication $C' = A'B'$ to have the quantized output C' . C' is subsequently approximated into C with a minimal overhead.

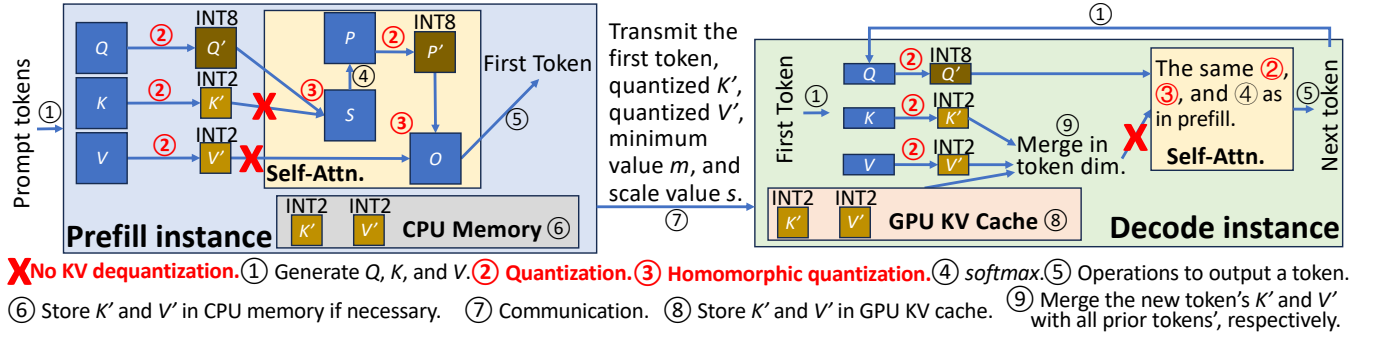


Figure 5: Overview of HACK in disaggregated LLM inference.

We use an asymmetric 2-bit stochastic quantization [31] to reduce quantization error, which partitions the elements of each row or column into partitions. Fig. 6 shows examples for partitioning. We denote the dimensions of the matrices A and B by $M \times Z$ and $Z \times N$, respectively. Fig. 6(a) illustrates quantization by partitioning elements in each row of A and each column of B . The quantization partition size, denoted by Π , is the number of elements in a partition. To increase accuracy, we can perform finer-grained quantization by setting a smaller Π , i.e., dividing the inner dimensions of the two matrices into more partitions. For example, Fig. 6(b) illustrates quantization by partitioning elements in half of a row of A and half of a column of B . In each partition i , the method identifies the minimum (\min_i) and maximum (\max_i) values of the matrix elements and computes the $\text{scale} = \frac{\max_i - \min_i}{2^2 - 1}$. Each original value x in a partition is quantized to an integer $x' = \text{round}(\frac{x - \min_i}{\text{scale}})$. The stochastic rounding $\text{round}(\ast)$ rounds \ast to $\lfloor \ast \rfloor$ with probability $(\lceil \ast \rceil - \ast) / (\lceil \ast \rceil - \lfloor \ast \rfloor)$ and to $\lceil \ast \rceil$ otherwise.

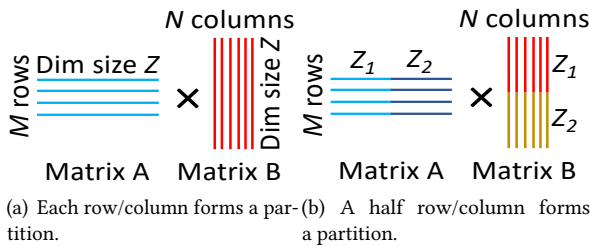


Figure 6: Illustration of partitioning for quantization.

Next, we need to estimate C given C' . For Fig. 6(a), let a_{iz} represent the element in the i -th row and z -th column of A , and b_{zj} represent the element in the z -th row and j -th column of B . The matrix multiplication $C = AB$ can then be expressed as $c_{ij} = \sum_{z=1}^Z a_{iz}b_{zj}$ for $i \in [1, M]$ and $j \in [1, N]$. Let m_{a_i} and s_{a_i} denote the minimum and scale values of a_{iz} . Since $a'_{iz} = \text{round}(\frac{a_{iz} - m_{a_i}}{s_{a_i}})$ and $b'_{zj} = \text{round}(\frac{b_{zj} - m_{b_j}}{s_{b_j}})$, we

have $a_{iz} \approx s_{a_i}q_{a_{iz}} + m_{a_i}$ and $b_{zj} \approx s_{b_j}q_{b_{zj}} + m_{b_j}$. Thus, $(AB)_{ij}$ can be extended to:

$$\sum_z a_{iz}b_{zj} \approx s_{a_i}s_{b_j} \sum_z a'_{iz}b'_{zj} + m_{b_j}s_{a_i} \sum_z a'_{iz} + m_{a_i}s_{b_j} \sum_z b'_{zj} + Zm_{a_i}m_{b_j}, \quad (4)$$

where $\{\sum_z a'_{iz}b'_{zj}, \forall i, j\}$ is the quantized matrix multiplication that can be accelerated by INT8 computation. The other terms in Eq. (4) approximate $\sum_z a'_{iz}b'_{zj}$ (C') into $\sum_z a_{iz}b_{zj}$ (C). Eq. (4) is the homomorphic quantization for multiplication.

We now analyze the computational cost of matrix multiplication and approximation in Eq. (4). The computational cost for $\sum_z a'_{iz}b'_{zj}$ is $2MZN$. The remaining cost for approximating $\sum_z a'_{iz}b'_{zj}$ into $\sum_z a_{iz}b_{zj}$ is $2MN$ for multiplying s_{a_i} , s_{b_j} , and $\sum_z a'_{iz}b'_{zj}$, $MN + MZ$ for $m_{b_j}s_{a_i} \sum_z a'_{iz}$, $MN + NZ$ for $m_{a_i}s_{b_j} \sum_z b'_{zj}$, $2MN$ for $Zm_{a_i}m_{b_j}$, and $3MN$ for adding all terms, totaling $9MN + MZ + NZ$.

For Fig. 6(b), AB can be viewed as $[A_1, A_2][B_1, B_2]^T$, which equals to $A_1B_1^T + A_2B_2^T$, where A_1, A_2, B_1 , and B_2 are blocks, and each of them has multiple partitions. The multiplications $A_1B_1^T$ and $A_2B_2^T$ are performed using Eq. (4), separately, followed by a summation to produce the result of AB .

5.3 Homomorphic Quantization in Disaggregated LLM Inference

We provide a detailed explanation of how our homomorphic quantization in Eq. (4) is applied to the self-attention in disaggregated LLM inference in Fig. 5. Fig. 7 shows an example. The inner dimension of Q and K is the head dimension of size d_h , and we divide this dimension into two partitions, so that Q and K both have two blocks, determined by the partition size Π . Π must be set as a multiple of 16 to ensure efficient execution of matrix operations on the underlying GPU hardware. Q and K are quantized for homomorphic quantization to output the attention score S , which will be processed to attention probability P via softmax in Eq. (3). The inner dimension of P and V is the sequence dimension

(denoted by L_{KV}) rather than the head dimension. We divide this sequence dimension into three parts so that P and V both have three blocks, which is determined by Π . P and V are quantized for homomorphic quantization to output O for token generation. During the prefill stage, the sequence lengths of Q (L_Q) and KV (L_{KV}) in Fig. 7 are identical, equaling to the number of prompt tokens. The prefill instance executes Eq. (2), during which $Q^h(K^h)^T$ and P^hV^h are calculated using Eq. (4). The prefill instance sends the first output token, the quantized K' and V' , the minimum values m , and the maximum values s to the decode instance. During the decode stage, $L_Q = 1$ for the single input token. The decode instance conduct the same process as the prefill instance. After a token is generated in an iteration, it appends the token's K' and V' to the previous K' and V' along the sequence dimension L_{KV} as shown in Fig. 7 and repeats the same process to generate the next token.

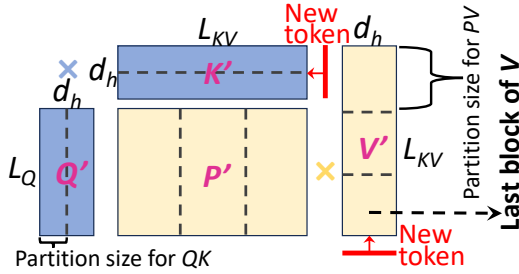


Figure 7: Illustration of partitioning in self-attention.

Summation elimination. We first analyze the overhead of approximation in homomorphic quantization during the decode stage and then explain how we reduce this overhead. As mentioned, in each decode iteration, matrices Q and K have $M = L_Q = 1$, $Z = d_h$, and $N = L_{KV}$; matrices P and V have $M = L_Q = 1$, $Z = L_{KV}$, and $N = d_h$. The approximation in Eq. (4) has the computational cost of $9MN + MZ + NZ$, as explained in §5.2, which means the cost of the approximation is $10(d_h + L_{KV}) + 2d_hL_{KV}$ in each decode iteration. If we do not use our homomorphic quantization, and we dequantize KV using the dequantization operation $sx' + m$ in every decode iteration, the cost for dequantizing KV is $2d_hL_{KV}$ for K and $2d_hL_{KV}$ for V , totaling $4d_hL_{KV}$. Our approximation overhead is $2d_hL_{KV} - 10(d_h + L_{KV})$ less than the overhead for dequantizing KV . In a decode iteration, since the summation term $\sum_z b'_{zj}$ for approximation in Eq. (4) has a cost of NZ , it leads to a cost of d_hL_{KV} for summing the elements in quantized K and a cost of d_hL_{KV} for summing the elements in quantized V , totaling $2d_hL_{KV}$, in each decode iteration. To reduce the summation computation, we store the sum $\sum_z b'_{zj}$ for K and V during decode and reuse them every iteration to avoid the recomputation cost. For a partition size of Π with b -bit integer quantization, the integer sum $\sum_z b'_{zj}$ requires

at most $b + \lceil \log_2 \Pi \rceil$ bits for storage. For example, for $\Pi = 64$ with 2-bit quantization, each partition needs at most eight bits to store a sum value. Therefore, we use $b + \lceil \log_2 \Pi \rceil$ bits to store the sum value. This only needs a little extra memory, up to $\sim 2.7\%$ of the GPU memory capacity (§7.4). Then, the final approximation cost is only $10(d_h + L_{KV})$ in each decode iteration. The head dimension size d_h is typically 128. Thus, the KV dequantization cost $4d_hL_{KV} > 10(d_h + L_{KV})$ when the sequence length $L_{KV} > 2.5$, and $4d_hL_{KV}$ exceeds $10(d_h + L_{KV})$ by an order of magnitude when the sequence length $L_{KV} > 30$. Therefore, when $L_{KV} > 30$, the approximation cost in Eq. (4) can be significantly reduced compared to the KV dequantization overhead in each decode iteration. The longer the sequence, the greater the reduction in the approximation cost.

Requantization elimination for the last block of V . After each decode iteration, the new token's KV values are appended to all prior tokens' KV values, as shown in Fig. 7. Since all the elements of a partition in K are arranged along the fixed head dimension, all the elements of the new token's K form one or more partitions by themselves. Hence, the $[\min, \max]$ of the previous K partitions won't be changed. In contrast, all the elements of a partition in V are arranged along the sequence dimension, which is incremented by 1 after each iteration. It means the elements of the new token's V will be distributed to the previous partitions. If the number of tokens in the last block of V (as shown in Fig. 7) is less than the partition size Π , each element of the new token's V on column j is added to the existing partition on column j . However, the element of the new token's V on column j may fall outside of the previous $[\min_j, \max_j]$ range, leading to the necessity of updating the range and scale s_j . Then, all other tokens' values on column j of the last block of V must be requantized. Fig. 8 illustrates an example of this. When the V of the new token $t+2$ is added to the last block of V , its value on the second column, -2.9 , falls outside the previous $[\min, \max]$ range $[-2.1, 1.7]$ of that column. Consequently, the \min needs to be updated to -2.9 , and all values on that column (-2.1 and 1.7) must be requantized based on the update $[\min, \max]$.

To do this, we could first dequantize old quantized values using the old \min_j and s_j , quantize them and the new value by the updated \min_j and s_j , and then perform the quantized matrix multiplication for the last block of P and the last block of V . However, this requantization

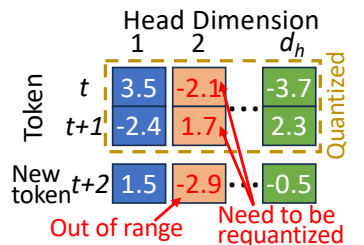


Figure 8: An example of requantization in the last block of V .

process not only increases the quantization error but also introduces extra overhead. To address this, we do not store the quantized values of the last group of V when its number of tokens does not reach the partition size Π . Instead, we store the original FP16 values for the last group of V in a cache separate from the quantized KV cache, which only occupies up to 0.51% of the GPU memory capacity (§7.4). The matrix multiplication for the last block of P and the last block of V are performed in FP16 format without quantization. When the number of tokens in the last block of V reaches Π , it is quantized and moved to the quantized KV cache. As the matrix multiplication in FP16 is restricted to the last block of V , the associated computation time with FP16 does not scale with sequence length.

6 IMPLEMENTATION

Attention backend. We integrated HACK with a widely adopted memory-efficient attention backend, FlashAttention-2 [18], by using OpenAI Triton [39] and a Triton-based implementation of FlashAttention-2 [43]. We built our system on top of vLLM [32] using the modified FlashAttention-2. Since Triton currently supports a minimum precision of INT8 for computation, we first convert the format of the quantized data from 2-bit into INT8 before performing matrix multiplication on the quantized data. This operation is performed in local GPU memory instead of global GPU memory, to reduce the overhead for accessing data.

Kernel fusion. We implemented two kernels using Triton: *attn_prefill*, used during the prefill stage, and *attn_decode*, used during the decode stage. To reduce overhead, *attn_prefill* fuses the generation of QKV, QKV quantization, and self-attention with homomorphic quantization into a single kernel. In addition to these three steps, *attn_decode* integrates the process of concatenating the new token’s quantized KV data with the previous tokens’ KV data into the kernel to further reduce overhead. In decode, *attn_decode* separates the last block of V from the quantized blocks into a buffer to enable the matrix multiplication with the original FP16 data.

Data management. To store the quantized KV data, along with their m , s , and sum value $\sum_z b'_{zj}$, we modified the KV cache structure of vLLM. Values m and s are stored in FP16. As mentioned in §5.3, we need $b + \lceil \log_2 \Pi \rceil$ bits to store the sum $\sum_z b'_{zj}$ for a quantization partition with b -bit quantization. However, this may lead to memory alignment issues for a certain combination of b and $|GS|$. For example, we need 9 bits to store a sum value for 2-bit quantization with a partition size of 128. The 9-bit value can not be stored in memory at addresses that align with the GPU’s natural boundaries. Therefore, we use INT16 to store a sum for this

case to address the issue with memory alignment. The memory required by the INT16 sum values only accounts for approximately 5% of the quantized KV data. The transmission of KV data between prefill instances and decode instances is implemented using NCCL [16].

7 PERFORMANCE EVALUATION

We evaluated HACK and present results in this section. The experimental setup is shown in §7.1. The comparison methods are the disaggregated LLM inference baseline, CacheGen and KVQaunt. HACK uses a partition size $\Pi=64$, achieving 0.16%-0.78% higher accuracy on average compared to CacheGen and KVQuant across all datasets and models.

7.1 Experiment Settings

Testbed. The AWS GPU instances used in this paper are listed in Table 2. Unless otherwise indicated, we used two p4de.24xlarge for decode [40, 52]; ten g5.12xlarge, sixteen p3.8xlarge, sixteen g4dn.12xlarge, ten g6.12xlarge, or two p4de.24xlarge for prefill so that prefill instances and decode instances have roughly similar capacities, avoiding underutilizing decode instances [40]. Since existing disaggregated LLM inference systems such as DistServe [52] and SplitWise [40] do not support Ethernet data transmission, we modified their code to enable it and integrated them onto vLLM [32] as a baseline. The RPS was set to the maximum processing capacity, following a Poisson distribution as in [52]. The prefill and decode requests were assigned to the respective prefill and decode instances with the shortest updated queue length [40], defined by the number of queuing tokens.

Name	GPUs	GPU memory	Bandwidth	vCPUs	Memory
g5.12xlarge	4 A10G	96 GiB	40 Gbps	48	192 GiB
p3.8xlarge	4 V100	64 GiB	10 Gbps	32	244 GiB
g4dn.12xlarge	4 T4	64 GiB	50 Gbps	48	192 GiB
g6.12xlarge	4 L4	96 GiB	40 Gbps	48	192 GiB
p4de.24xlarge	8 A100	640 GiB	400 Gbps	96	1152 GiB

Table 2: GPU instances.

Model	A10G, L4	V100, T4	A100
Mistral-v0.3 7B (M)	TP=4, no PP	TP=4, no PP	no TP, no PP
Phi-3 14B (P)	TP=2, PP=2	TP=2, PP=2	no TP, no PP
Yi 34B (Y)	TP=4, PP=2	TP=4, PP=2	TP=4, no PP
Llama-3.1 70B (L)	TP=4, PP=2	TP=4, PP=4	TP=4, no PP
Falcon 180B (F)	TP=4, PP=5	TP=4, PP=8	TP=4, PP=2

Table 3: TP and PP degrees.

Models and datasets. We used a range of state-of-the-art models in the paper: Mistral AI Mistral-v0.3 7B [7], Microsoft

Dataset	Input length			Output length		
	avg	min	max	avg	min	max
IMDb classification [26]	315	106	821	37	16	87
arXiv summarization [15]	6.3K	1.6K	14.1K	243	29	464
Cocktail for IR [17]	16.2K	9.4K	28.8K	159	44	246
HumanEval [13]	204	75	697	139	11	552

Table 4: Dataset properties.

Phi-3 14B [6], 01-ai Yi 34B [1], Meta Llama-3.1 70B [5], and TII Falcon 180B [3]. We use the initial letters M, P, Y, L, and F to represent each model, respectively, for the rest of the paper. Table 3 shows the Tensor Parallelism (TP) and Pipeline Parallelism (PP) degree of each model in different GPU instances, following practical configurations to ensure sufficient GPU memory to handle requests [40, 52]. The datasets we use are listed in Table 4. IMDb includes 27 genres of movies, TV shows, etc., collected on the Internet. It is operated by IMDb.com, Inc., a subsidiary of Amazon. The arXiv summarization has a collection of scientific publications and their summaries on arXiv.org [12]. Information Retrieval (IR) is the process of retrieving relevant content from vast amounts of information based on a user query. Cocktail is a benchmark for IR, including 8 different IR tasks such as question answering, fact checking, etc. HumanEval evaluates the performance of code completion, including 164 programming problems. We use *ROUGE-1* [35] and *Edit Similarity (normalized Levenshtein distance)* [46, 50] as the accuracy metric for arXiv summarization and HumanEval, respectively. Unless otherwise specified, we default to testing with the Llama-3.1 70B model and the Cocktail dataset with long sequences on A10G prefill instances, which have the same architecture as the A100.

7.2 End-to-End Time Performance

We tested Llama-3.1 70B on A10 prefill instances across different datasets. Fig. 9 shows the average JCT across all requests. For IMDb, HumanEval, arXiv, and Cocktail, HACK reduces the average JCT by 19.2%, 22.5%, 36.8%, and 41.5%, respectively, compared to CacheGen, and by 21.2%, 25.1%, 40.8%, and 45.1%, respectively, compared to KVQuant. This is because HACK leverages quantized matrix multiplication, accelerating both prefill and decode stages while eliminating KV dequantization overhead. For IMDb, HumanEval, arXiv, and Cocktail, HACK reduces the average JCT by 38.6%, 40.1%, 55.3%, and 61.6%, respectively, compared to the baseline. This improvement is due to HACK not only accelerating prefill and decode stages but also reducing KV transmission overhead. The improvement in JCT achieved by HACK for arXiv and Cocktail is higher than IMDb and HumanEval because arXiv and Cocktail have longer sequences.

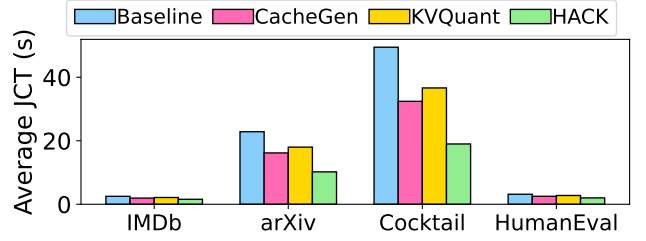


Figure 9: Average JCT across requests for Llama-3.1 70B with varying datasets.

We decompose the average JCT in Fig. 9 into prefill, quantization, KV communication, dequantization/approximation, and decode time, as shown in Fig. 10. The approximation time in homomorphic quantization is only for HACK, and the dequantization time is for other methods. For IMDb, HumanEval, arXiv, and Cocktail, HACK achieves lower prefill times than other methods by 14.6%-23.7%, 17.5%-23.4%, 34.2%-37.5%, and 35.9%-41.9%, respectively. This is due to the acceleration of prefill computation via quantized matrix multiplication in Eq. (4). The longer the sequence, the greater the improvement in prefill time. The quantization overhead for CacheGen, KVQuant, and HACK accounts for only 1.25%-2.91% of JCT, as the quantization of KV data for each token occurs only once during the entire end-to-end process. By compressing KV data to approximately 15% of its original size, HACK, CacheGen, and KVQuant reduce KV transmission time by 80.6%-85.4% compared to the baseline, enabling KV transmission to account for only 1.31%-5.4% of JCT. HACK eliminates the KV dequantization overhead, which accounts for 17.2%-30.4% of JCT in CacheGen and KVQuant, replacing it with only 1.53%-3.18% overhead for approximation in homomorphic quantization.

For IMDb, HumanEval, arXiv, and Cocktail, HACK reduces the decode time by 11.5%-12.2%, 13.7%-14.5%, 24.3%-25.6%, and 32.1%-33.7% compared to CacheGen and KVQuant, due to accelerated computation from quantized matrix multiplication. For short-sequence datasets IMDb and HumanEval, the improvement in decode time is only 11.5%-14.5% because the number of tokens in the last block of V has a high proportion in the sequence length, which leads to compromised efficiency with FP16 computation. The improvement in decode time for long-sequence datasets arXiv, and Cocktail is around 20% higher than IMDb and HumanEval because the proportion of the number of tokens of the last block of V in the sequence length is small, and thus, the quantized matrix multiplication benefits the decode time more. CacheGen and KVQuant reduce decode time by 16.5%-38.1% compared to the baseline because the reduced KV size improves the

memory access latency. HACK also benefits from the improvement in memory access latency. HACK is effective in reducing JCT for different datasets.

Table 5 lists the peak GPU memory usage on decode instances for different datasets. CacheGen, KVQuant, and HACK can reduce the peak GPU memory usage by 13.9%-19.6% for short-sequence datasets IMDb and HumanEval and by 25.0%-33.6% for long-sequence datasets. HACK has 0.6% and 2.9% higher peak GPU memory usage because it stores the sum value for the approximation step in homomorphic quantization and stores the FP16 data for the last block of V .

	IMDb	arXiv	Cocktail	HumanEval
Baseline	65.3%	83.1%	93.7%	68.9%
CacheGen	49.6%	56.2%	61.3%	50.8%
KVQuant	48.5%	55.9%	60.1%	49.3%
HACK	51.4%	58.1%	63.0%	51.4%

Table 5: Peak GPU memory usage on decode instances with varying datasets.

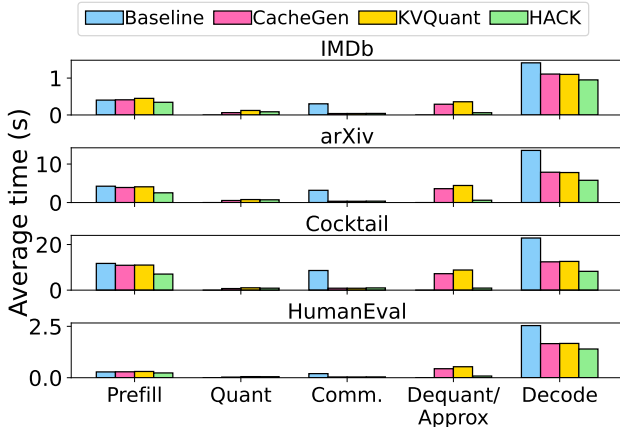


Figure 10: Average JCT decomposition for Llama-3.1 70B with varying datasets.

We also tested different models with the Cocktail using A10G prefill instances. Fig. 11 shows the average JCT across all requests. For M, P, Y, L, and F-arXiv, HACK reduces the average JCT by 42.4%, 39.1%, 44.8%, 41.5%, and 31.7%, respectively, compared to CacheGen. HACK reduces the average JCT by 48.3%, 46.5%, 50.7%, 45.1%, and 37.6%, respectively, compared to KVQuant. Compared to the baseline, HACK reduces it by 54.6%, 57.2%, 58.7%, 61.6%, and 53.3%, respectively. The reasons are the same as those discussed in Fig. 9. HACK’s improvement on F-arXiv is smaller than that for other models because the sequence length used in F-arXiv is shorter, capped at 2K. HACK is effective in reducing JCT for different models.

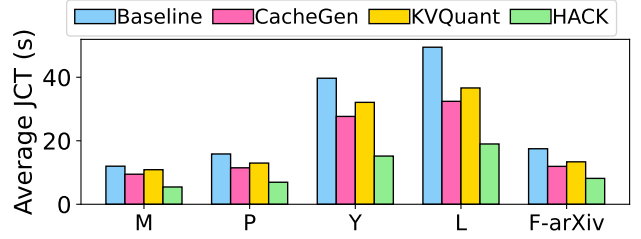


Figure 11: Average JCT across requests for different models with Cocktail or arXiv.

We tested Llama-3.1 70B with the Cocktail on different prefill instances, and Fig. 12 shows the average JCT across all requests under different prefill instances. For A10G, V100, T4, L4, and A100, HACK reduces the average JCT compared to CacheGen by 41.5%, 37.4%, 43.1%, 45.3%, and 48.5%; compared to KVQuant by 45.1%, 41.7%, 46.6%, 50.5%, and 52.3%; and compared to the baseline by 61.6%, 70.9%, 62.1%, 59.3%, and 60.5%, respectively. The improvement of HACK over CacheGen and KVQuant on V100 is the smallest because the V100 tensor core does not support INT8 matrix multiplication, making it unable to accelerate prefill computation. However, HACK achieves the highest improvement over the baseline on V100, as V100 has the lowest bandwidth, and HACK significantly improves the KV transmission speed. HACK is effective in reducing JCT for various prefill instances with various bandwidths and compute capacity.

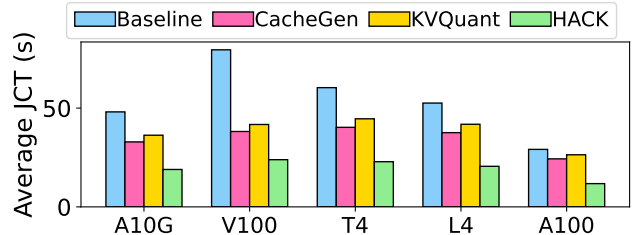


Figure 12: Average JCT across requests for Llama-3.1 70B with Cocktail using varying prefill instances.

7.3 Accuracy Performance

We measured the accuracy of each method across different datasets and models, as shown in Table 6. HACK uses three partition sizes $\Pi=128$, 64, and 32, denoted by HACK ($\Pi=128$), HACK ($\Pi=64$), and HACK ($\Pi=32$). Compared to the baseline, HACK ($\Pi=32$), HACK ($\Pi=64$), CacheGen, KVQuant, and HACK ($\Pi=128$) exhibit accuracy losses of 0.55%-1.17%, 0.76%-1.56%, 1.44%-2.08%, 1.46%-2.33%, and 1.37%-2.68%, respectively. HACK ($\Pi=32$) and HACK ($\Pi=64$) achieve higher accuracy than CacheGen and KVQuant due to the fine-grained partition size. Meanwhile, HACK ($\Pi=128$) has a 0.21%-1.27%

	IMDb					arXiv					Cocktail				HumanEval				
	M	P	Y	L	F	M	P	Y	L	F	M	P	Y	L	M	P	Y	L	F
Baseline	84.81%	87.84%	93.87%	95.73%	85.63%	79.40%	86.35%	87.75%	83.79%	79.42%	75.18%	83.92%	85.25%	86.39%	89.37%	91.62%	90.79%	92.45%	85.21%
HACK ($\Pi=32$)	83.79%	87.08%	92.82%	94.73%	84.96%	78.53%	85.51%	86.69%	82.63%	78.75%	74.63%	83.05%	84.39%	85.54%	88.68%	90.50%	90.02%	91.28%	84.26%
HACK ($\Pi=64$)	83.46%	86.64%	92.31%	94.17%	84.72%	78.26%	85.08%	86.39%	82.31%	78.28%	74.42%	82.66%	84.04%	84.87%	88.19%	90.16%	89.63%	91.04%	83.82%
CacheGen	83.04%	86.15%	91.79%	93.85%	83.94%	77.87%	84.62%	86.02%	82.14%	77.85%	73.74%	82.24%	83.51%	84.71%	87.73%	89.75%	88.94%	90.49%	83.47%
KVQuant	82.97%	86.05%	91.54%	93.89%	84.12%	77.83%	84.65%	86.11%	82.08%	77.76%	73.72%	82.26%	83.42%	84.68%	87.64%	89.65%	88.93%	90.43%	83.29%
HACK ($\Pi=128$)	82.71%	86.07%	91.35%	93.76%	84.03%	77.72%	84.49%	86.15%	81.97%	77.94%	73.81%	82.19%	82.86%	84.65%	87.60%	89.54%	88.91%	89.77%	83.19%

Table 6: Accuracy performance.

lower accuracy than HACK ($\Pi=128$) due to the larger partition size and has a slightly lower accuracy than KVQuant on average, by no more than 0.12%. Across different models and datasets, all methods exhibit similar accuracy loss trends. Since the partition size of 64 is enough for HACK to have better accuracy than CacheGen and KVQuant, we use $\Pi=64$ as the default partition size for HACK in the evaluation.

7.4 Ablation Study

We conducted ablation study to understand the impact of two of our optimizations on end-to-end performance and accuracy: the summation elimination for Eq. (4) and requantization elimination for the last block of V . We tested the following variations. HACK/SE represents HACK without *Summation Elimination*, which means it does not store the term $\sum_z b_{zj}$ in Eq. (4) and recomputes it every decode iteration. HACK/RQE represents the system without *ReQuantization Elimination* for the last block of V , and instead checks and requantizes the last block of V every decode iteration. Fig. 13 shows the average JCT across all requests for HACK, HACK/SE, and HACK/RQE when varying datasets. HACK/SE has 13.8%-15.3% higher average JCT for the short-sequence datasets (IMDb and HumanEval) and has 22.1%-25.9% higher average JCT for the long-sequence datasets (arXiv and Cocktail) compared to HACK. Long sequences increase the overhead in recomputing the sum value $\sum_z b_{zj}$ for KV. HACK/RQE has 17.8%-21.7% higher average JCT for the short-sequence datasets and has 0.09%-1.2% higher average JCT for the long-sequence datasets compared to HACK. As the sequence length increases, the proportion of tokens in the last block of V compared to the total number of tokens decreases, making the overhead of requantizing the last block of V comparatively smaller. Table 7 lists the decrease in accuracy for HACK/RQE compared to HACK under different datasets. Since the quantization error caused by requantization of the last block of V is only accumulated during the decode stage, the accuracy decrease is affected by the output length. IMDb has an average output length of 37, while others have an average output length of 139-243. Thus, IMDb has a 0.08%-0.15% less decrease in accuracy than other

datasets. SE is effective in reducing the summation overhead, and RQE can avoid accuracy loss without compromising the end-to-end performance.

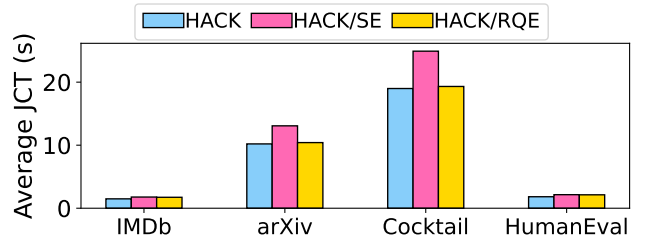


Figure 13: Average JCT across requests for individual methods with Llama-3.1 70B.

IMDb	arXiv	Cocktail	HumanEval
-0.14%	-0.29%	-0.22%	-0.25%

Table 7: The decrease in accuracy for HACK/RQE compared to HACK.

For SE, storing the sum values $\sum_z b_{zj}$ in Eq. (4) for KV to avoid redundant computation only requires 2.2%-2.7% of GPU memory capacity in the experiment. For RQE, storing the FP16 values for the last block of V only requires 0.24%-0.51% of GPU memory capacity.

7.5 Sensitivity Testing

We investigated the impact of HACK’s different quantization partition sizes on end-to-end performance for Llama-3.1 70B on A10G prefill instances with different datasets. Table. 8 lists the increase in accuracy and the percentage increase in the average JCT across all requests for quantization partition sizes $\Pi=32$ and $\Pi=64$ compared to $\Pi=128$. While $\Pi=32$ achieves the highest accuracy with up to 1.53% increase, it can increase the average JCT by up to 28%, which means it is a trade-off between accuracy and end-to-end performance requirements.

	IMDb		arXiv		Cocktail		HumanEval	
	Acc.	JCT	Acc.	JCT	Acc.	JCT	Acc.	JCT
$\Pi=32$	0.92-1.46%	17.1%	0.53-1.02%	25.2%	0.81-1.53%	28%	0.95-1.51%	13.8%
$\Pi=64$	0.4-0.96%	5.9%	0.23-0.59%	8.3%	0.22-1.18%	9.2%	0.59-1.27%	5.1%

Table 8: The increase in accuracy and average JCT across requests compared to $\Pi=128$.

7.6 Scalability Testing

We then test the ability of HACK to mitigate network bottlenecks using Llama-3.1 70B and Cocktail. We use p to denote the ratio of the number of model replicas for prefill to the number of model replicas for decode. The decode model ran on an A100 instance, and due to TP=4, only half of the A100 instance’s GPU and network resources (i.e., 4 GPUs and a 200Gbps network) were allocated to serve it. The model replicas for prefill ran on A10G instances, and with TP=4 and PP=2, each prefill model required two A10G instances to serve it. The RPS was set to $0.02p$. Fig. 14 shows the average JCT across all requests when p increases from 1 to 8. When p increases from 1 to 8, the baseline’s average JCT increases by 127%, whereas CacheGen, KVQuant, and HACK only have an increase of 31-43%. This demonstrates that CacheGen, KVQuant, and HACK effectively reduce the overhead caused by KV transmission at large scales.

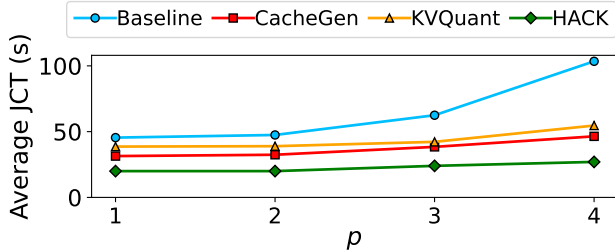


Figure 14: Average JCT across requests with varying p .

8 LIMITATIONS AND FUTURE WORK

Since one of our focuses is on mitigating the KV transmission bottleneck in disaggregated LLM inference, we employ 2-bit quantization to minimize KV transmission overhead. However, due to the low precision of 2-bit quantization, we must use small partition sizes to improve accuracy, which can increase JCT. To address this, we plan to explore new quantization schemes that can reduce JCT and improve accuracy in disaggregated LLM inference in the future. Additionally, since Triton only supports INT8 computation and incurs runtime overhead, we intend to implement HACK directly in CUDA to support INT4 computation and reduce execution overhead in our future work.

9 RELATED WORK

Homomorphic Compression. The concept of homomorphic compression, where arithmetic operations are performed directly on compressed data, has been explored in the context of gradient aggregation [34], enabling a parameter server to aggregate compressed gradients without decompressing them. However, this method is limited to addition operations and is unsuitable for the matrix multiplications required in the attention computation procedure.

Disaggregated LLM inference. Disaggregated LLM inference [24, 40–42, 52] has gained popularity as it separates the computation-intensive prefill and memory-intensive decode stages into different instances, improving resource utilization. Two works [40, 42, 52] focus on disaggregated LLM inference systems. Other research [24, 41] focuses on KV cache sharing, where KV data generated during the prefill stage is stored and shared across requests to reduce computation time. However, transmitting KV values from the prefill instance to the decode instance can become a bottleneck, a challenge that intensifies with KV data sharing. Our work addresses this issue by introducing homomorphic quantization, eliminating significant KV dequantization overhead.

KV Quantization. Many methods use quantization to compress KV [22, 23, 29, 36, 38] by reducing the high-bit representation FP16 to lower-bit representations in order to reduce the size of KV data. However, during attention computation, the quantized KV in the KV cache must first be dequantized to recover the original data, introducing significant decompression overhead. HACK, on the other hand, uses homomorphic quantization to avoid the KV dequantization overhead and performs attention computation on low-precision data to accelerate speed.

Recent work TurboAttention [28] on arXiv, also performs attention computation directly on quantized KV data; however, it focuses solely on accelerating computation and mitigating KV cache bottlenecks. In contrast, our work not only accelerates computation and mitigates KV cache bottlenecks but also focuses on minimizing KV communication overhead in disaggregated LLM inference by leveraging 2-bit quantization. Furthermore, TurboAttention chooses symmetric quantization to reduce computation overhead, which has a lower accuracy than asymmetric quantization [28]. HACK uses asymmetric quantization with summation elimination to increase accuracy. In addition, HACK eliminates the re-quantization overhead and reduce quantization error for the last block of V during the decode stage.

KV Eviction. Another solution for KV compression is KV eviction [9, 11, 19, 20, 27, 33, 37, 48, 49, 51], also known as KV pruning, which removes unimportant tokens’ KV that

have minimal impact on inference results, measured by attention scores. Eviction-based methods and quantization-based methods are complementary: the former reduces the number of elements in the KV matrix, while the latter lowers the precision of those elements. These two approaches can be combined for enhanced effectiveness. While our work focuses on homomorphic quantization, we plan to explore how KV eviction can address the challenges in future work.

10 CONCLUSION

HACK is a novel quantization method for disaggregated LLM inference, which reduces the KV transmission overhead, computation time, and memory access latency for KV without introducing the expensive KV dequantization overhead. We integrate HACK into a widely adopted memory-efficient attention kernel, FlashAttention-2, and build our system on vLLM. We conduct extensive experiments to demonstrate the efficiency of HACK, where HACK can reduce JCT by up to 70.9% due to the improvement in communication, computation, memory access latency, and the elimination of KV dequantization. This work does not raise any ethical issues.

REFERENCES

- [1] 2025. 01-ai Model Yi. <https://huggingface.co/01-ai/Yi-34B-200K>. (2025).
- [2] 2025. The code of HKVQ. <https://anonymous.4open.science/r/HKVQ>. (2025).
- [3] 2025. Falcon-180B. <https://huggingface.co/tiiuae/falcon-180B>. (2025).
- [4] 2025. GPT-4 explaining Self-Attention Mechanism. <https://www.linkedin.com/pulse/gpt-4-explaining-self-attention-mechanism-fatos-ismali/>. (2025).
- [5] 2025. Meta Llama-3.1. <https://llama.meta.com/>. (2025).
- [6] 2025. Microsoft Phi-3. <https://huggingface.co/microsoft/Phi-3-medium-128k-instruct>. (2025).
- [7] 2025. Mistral-v0.3. <https://huggingface.co/mistralai/Mistral-7B-Instruct-v0.3>. (2025).
- [8] 2025. Open Compute Project. <https://www.opencompute.org/documents/ocp-microscaling-formats-mx-v1-0-spec-final-pdf>. (2025).
- [9] Muhammad Adnan, Akhil Arunkumar, Gaurav Jain, Prashant Nair, Ilya Soloveychik, and Purushotham Kamath. 2024. Keyformer: KV Cache reduction through key tokens selection for Efficient Generative Inference. In *Proceedings of Machine Learning and Systems*, P. Gibbons, G. Pekhimenko, and C. De Sa (Eds.), Vol. 6. 114–127. https://proceedings.mlsys.org/paper_files/paper/2024/file/48fecef47b19fe501d27d338b6d52582-Paper-Conference.pdf
- [10] Inc. Amazon Web Services. 2024. Recommended AWS GPU Instances. <https://docs.aws.amazon.com/dlami/latest/devguide/gpu.html>. (2024).
- [11] Sotiris Anagnostidis, Dario Pavllo, Luca Biggio, Lorenzo Noci, Aurelien Lucchi, and Thomas Hofmann. 2023. Dynamic Context Pruning for Efficient and Interpretable Autoregressive Transformers. In *Advances in Neural Information Processing Systems*, A. Oh, T. Naumann, A. Globerson, K. Saenko, M. Hardt, and S. Levine (Eds.), Vol. 36. Curran Associates, Inc., 65202–65223. https://proceedings.neurips.cc/paper_files/paper/2023/file/cdaac2a02c4fdcae77ba083b110efcc3-Paper-Conference.pdf
- [12] arXiv. 2025. arXiv. <https://arxiv.org>. (2025). Accessed: 2025-01-30.
- [13] Mark Chen, Jerry Tworek, Heewoo Jun, Qiming Yuan, Henrique Ponde de Oliveira Pinto, Jared Kaplan, Harri Edwards, Yuri Burda, Nicholas Joseph, Greg Brockman, Alex Ray, Raul Puri, Gretchen Krueger, Michael Petrov, Heidy Khlaaf, Girish Sastry, Pamela Mishkin, Brooke Chan, Scott Gray, Nick Ryder, Mikhail Pavlov, Alethea Power, Lukasz Kaiser, Mohammad Bavarian, Clemens Winter, Philippe Tillet, Felipe Petroski Such, Dave Cummings, Matthias Plappert, Fotios Chantzis, Elizabeth Barnes, Ariel Herbert-Voss, William Hebgen Guss, Alex Nichol, Alex Paino, Nikolas Tezak, Jie Tang, Igor Babuschkin, Suchir Balaji, Shantanu Jain, William Saunders, Christopher Hesse, Andrew N. Carr, Jan Leike, Josh Achiam, Vedant Misra, Evan Morikawa, Alec Radford, Matthew Knight, Miles Brundage, Mira Murati, Katie Mayer, Peter Welinder, Bob McGrew, Dario Amodei, Sam McCandlish, Ilya Sutskever, and Wojciech Zaremba. 2021. Evaluating Large Language Models Trained on Code. (2021). arXiv:cs.LG/2107.03374 <https://arxiv.org/abs/2107.03374>
- [14] Tencent Cloud. 2024. Tencent Cloud - A100 Instances. <https://www.tencentcloud.com/document/product/560/19701#GT4>. (2024).
- [15] Arman Cohan, Franck Dernoncourt, Doo Soon Kim, Trung Bui, Seokhwan Kim, Walter Chang, and Nazli Goharian. 2018. A Discourse-Aware Attention Model for Abstractive Summarization of Long Documents. (2018). arXiv:cs.CL/1804.05685 <https://arxiv.org/abs/1804.05685>
- [16] NVIDIA Corporation. 2025. NVIDIA NCCL Documentation. <https://docs.nvidia.com/deeplearning/nccl/index.html>. (2025).
- [17] Sunhao Dai, Weihao Liu, Yuqi Zhou, Liang Pang, Rongju Ruan, Gang Wang, Zhenhua Dong, Jun Xu, and Ji-Rong Wen. 2024. Cocktail: A Comprehensive Information Retrieval Benchmark with LLM-Generated Documents Integration. (2024). arXiv:cs.IR/2405.16546 <https://arxiv.org/abs/2405.16546>
- [18] Tri Dao. 2023. FlashAttention-2: Faster Attention with Better Parallelism and Work Partitioning. (2023). arXiv:cs.LG/2307.08691 <https://arxiv.org/abs/2307.08691>
- [19] Alessio Devoto, Yu Zhao, Simone Scardapane, and Pasquale Minervini. 2024. A Simple and Effective L_2 Norm-Based Strategy for KV Cache Compression. In *Proceedings of the 2024 Conference on Empirical Methods in Natural Language Processing*, Yaser Al-Onaizan, Mohit Bansal, and Yun-Nung Chen (Eds.). Association for Computational Linguistics, Miami, Florida, USA, 18476–18499. <https://doi.org/10.18653/v1/2024.emnlp-main.1027>
- [20] Suyu Ge, Yunan Zhang, Liyuan Liu, Minjia Zhang, Jiawei Han, and Jianfeng Gao. 2023. Model tells you what to discard: Adaptive kv cache compression for llms. *arXiv preprint arXiv:2310.01801* (2023).
- [21] Google. 2024. Gemini 1.5. <https://gemini.google.com/app>. (2024).
- [22] Yefei He, Luoming Zhang, Weijia Wu, Jing Liu, Hong Zhou, and Bohan Zhuang. 2024. ZipCache: Accurate and Efficient KV Cache Quantization with Salient Token Identification. (2024). arXiv:cs.LG/2405.14256 <https://arxiv.org/abs/2405.14256>
- [23] Coleman Richard Charles Hooper, Sehoon Kim, Hiva Mohammadzadeh, Michael W. Mahoney, Sophia Shao, Kurt Keutzer, and Amir Gholami. 2024. KVQuant: Towards 10 Million Context Length LLM Inference with KV Cache Quantization. In *The Thirty-eighth Annual Conference on Neural Information Processing Systems*. <https://openreview.net/forum?id=0LXotew9Du>
- [24] Cunchen Hu, Heyang Huang, Junhao Hu, Jiang Xu, Xusheng Chen, Tao Xie, Chenxi Wang, Sa Wang, Yungang Bao, Ninghui Sun, and Yizhou Shan. 2024. MemServe: Context Caching for Disaggregated LLM Serving with Elastic Memory Pool. (2024). arXiv:cs.DC/2406.17565 <https://arxiv.org/abs/2406.17565>
- [25] Cunchen Hu, Heyang Huang, Liangliang Xu, Xusheng Chen, Jiang Xu, Shuang Chen, Hao Feng, Chenxi Wang, Sa Wang, Yungang Bao, Ninghui Sun, and Yizhou Shan. 2024. Inference without Interference:

- Disaggregate LLM Inference for Mixed Downstream Workloads. (2024). arXiv:cs.DC/2401.11181 <https://arxiv.org/abs/2401.11181>
- [26] IMDb. 2020. Genre Classification Dataset IMDb. <https://www.kaggle.com/datasets/hijest/genre-classification-dataset-imdb>. (2020).
- [27] Huiqiang Jiang, YUCHENG LI, Chengruidong Zhang, Qianhui Wu, Xufang Luo, Surin Ahn, Zhenhua Han, Amir H. Abdi, Dongsheng Li, Chin-Yew Lin, Yuqing Yang, and Lili Qiu. 2024. MInference 1.0: Accelerating Pre-filling for Long-Context LLMs via Dynamic Sparse Attention. In *The Thirty-eighth Annual Conference on Neural Information Processing Systems*. <https://openreview.net/forum?id=fPBACAbqSN>
- [28] Hao Kang, Srikant Bharadwaj, James Hensman, Tushar Krishna, Victor Ruhle, and Saravan Rajmohan. 2024. TurboAttention: Efficient Attention Approximation For High Throughputs LLMs. (2024). arXiv:cs.LG/2412.08585 <https://arxiv.org/abs/2412.08585>
- [29] Hao Kang, Qingru Zhang, Souvik Kundu, Geonhwa Jeong, Zaoxing Liu, Tushar Krishna, and Tuo Zhao. 2024. GEAR: An Efficient KV Cache Compression Recipe for Near-Lossless Generative Inference of LLM. *arXiv preprint arXiv:2403.05527* (2024). arXiv:cs.LG/2403.05527
- [30] Philip Kiely. 2024. NVIDIA A10 vs A10G for ML model inference. <https://www.baseten.co/blog/nvidia-a10-vs-a10g-for-ml-model-inference/>. (2024).
- [31] John R. Klauder. 1983. Stochastic Quantization. In *Recent Developments in High-Energy Physics*, H. Mitter and C. B. Lang (Eds.). Springer Vienna, Vienna, 251–281.
- [32] Woosuk Kwon, Zhuohan Li, Siyuan Zhuang, Ying Sheng, Lianmin Zheng, Cody Hao Yu, Joseph Gonzalez, Hao Zhang, and Ion Stoica. 2023. Efficient Memory Management for Large Language Model Serving with PagedAttention. In *Proceedings of the 29th Symposium on Operating Systems Principles (SOSP '23)*. Association for Computing Machinery, New York, NY, USA, 611–626. <https://doi.org/10.1145/3600006.3613165>
- [33] Wonbeom Lee, Jungi Lee, Junghwan Seo, and Jaewoong Sim. 2024. InfiGen: Efficient Generative Inference of Large Language Models with Dynamic KV Cache Management. In *18th USENIX Symposium on Operating Systems Design and Implementation (OSDI 24)*. USENIX Association, Santa Clara, CA, 155–172. <https://www.usenix.org/conference/osdi24/presentation/lee>
- [34] Minghao Li, Ran Ben Basat, Shay Vargafik, ChonLam Lao, Kevin Xu, Michael Mitzenmacher, and Minlan Yu. 2024. THC: Accelerating Distributed Deep Learning Using Tensor Homomorphic Compression. In *21st USENIX Symposium on Networked Systems Design and Implementation (NSDI 24)*. USENIX Association, Santa Clara, CA, 1191–1211. <https://www.usenix.org/conference/nsdi24/presentation/li-minghao>
- [35] Chin-Yew Lin. 2004. Rouge: A package for automatic evaluation of summaries. In *Text summarization branches out*. 74–81.
- [36] Yuhan Liu, Hanchen Li, Yihua Cheng, Siddhant Ray, Yuyang Huang, Qizheng Zhang, Kuntai Du, Jiayi Yao, Shan Lu, Ganesh Ananthanarayanan, Michael Maire, Henry Hoffmann, Ari Holtzman, and Junchen Jiang. 2024. CacheGen: KV Cache Compression and Streaming for Fast Large Language Model Serving. In *Proceedings of the ACM SIGCOMM 2024 Conference (ACM SIGCOMM '24)*. Association for Computing Machinery, New York, NY, USA, 38–56. <https://doi.org/10.1145/3651890.3672274>
- [37] Zichang Liu, Aditya Desai, Fangshuo Liao, Weitao Wang, Victor Xie, Zhaozhuo Xu, Anastasios Kyrillidis, and Anshumali Shrivastava. 2023. Scissorhands: Exploiting the Persistence of Importance Hypothesis for LLM KV Cache Compression at Test Time. In *Advances in Neural Information Processing Systems*, A. Oh, T. Neumann, A. Globerson, K. Saenko, M. Hardt, and S. Levine (Eds.), Vol. 36. Curran Associates, Inc., 52342–52364. https://proceedings.neurips.cc/paper_files/paper/2023/file/a452a7c6c463e4ae8fbd614c6e983e6-Paper-Conference.pdf
- [38] Zirui Liu, Jiayi Yuan, Hongye Jin, Shaochen Zhong, Zhaozhuo Xu, Vladimir Braverman, Beidi Chen, and Xia Hu. 2024. KIVI: A Tuning-Free Asymmetric 2bit Quantization for KV Cache. In *Proceedings of the 41st International Conference on Machine Learning (Proceedings of Machine Learning Research)*, Ruslan Salakhutdinov, Zico Kolter, Katherine Heller, Adrian Weller, Nuria Oliver, Jonathan Scarlett, and Felix Berkenkamp (Eds.), Vol. 235. PMLR, 32332–32344. <https://proceedings.mlr.press/v235/liu24bz.html>
- [39] OpenAI. 2021. Introducing Triton: Open-source GPU programming for neural networks. <https://openai.com/index/triton/>. (2021).
- [40] Pratyush Patel, Esha Choukse, Chaojie Zhang, Aashaka Shah, Íñigo Goiri, Saeed Maleki, and Ricardo Bianchini. 2024. Splitwise: Efficient Generative LLM Inference Using Phase Splitting. In *2024 ACM/IEEE 51st Annual International Symposium on Computer Architecture (ISCA)*. 118–132. <https://doi.org/10.1109/ISCA59077.2024.00019>
- [41] Ruoyu Qin, Zheming Li, Weiran He, Mingxing Zhang, Yongwei Wu, Weimin Zheng, and Xinran Xu. 2024. Mooncake: A KVCache-centric Disaggregated Architecture for LLM Serving. (2024). arXiv:cs.DC/2407.00079 <https://arxiv.org/abs/2407.00079>
- [42] Foteini Strati, Sara Mcallister, Amar Phanishayee, Jakub Tarnawski, and Ana Klimovic. 2024. DéjàVu: KV-cache Streaming for Fast, Fault-tolerant Generative LLM Serving. In *Proceedings of the 41st International Conference on Machine Learning (Proceedings of Machine Learning Research)*, Ruslan Salakhutdinov, Zico Kolter, Katherine Heller, Adrian Weller, Nuria Oliver, Jonathan Scarlett, and Felix Berkenkamp (Eds.), Vol. 235. PMLR, 46745–46771. <https://proceedings.mlr.press/v235/strati24a.html>
- [43] Philippe Tillet. 2020. Fused Attention in Triton. <https://triton-lang.org/main/getting-started/tutorials/06-fused-attention.html>. (2020).
- [44] vLLM Team. 2024. vLLM FP8 for KV Cache. https://docs.vllm.ai/en/v0.5.4/quantization/fp8_e4m3_kvcache.html. (2024).
- [45] Jie Wang, Huanxi Liu, Dawei Feng, Jie Ding, and Bo Ding. 2024. FP4-Quantization: Lossless 4bit Quantization for Large Language Models. In *2024 IEEE International Conference on Joint Cloud Computing (JCC)*. 61–67. <https://doi.org/10.1109/JCC62314.2024.00017>
- [46] Gang Wu. 2024. String Similarity Metrics – Edit Distance. <https://www.baeldung.com/cs/string-similarity-edit-distance>. (2024).
- [47] Haojun Xia, Zhen Zheng, Xiaoxia Wu, Shiyang Chen, Zhewei Yao, Stephen Youn, Arash Bakhtiari, Michael Wyatt, Donglin Zhuang, Zhongzhu Zhou, Olatunji Ruwase, Yuxiong He, and Shuaiwen Leon Song. 2024. FP6-LLM: Efficiently Serving Large Language Models Through FP6-Centric Algorithm-System Co-Design. (2024). arXiv:cs.LG/2401.14112 <https://arxiv.org/abs/2401.14112>
- [48] Dongjie Yang, XiaoDong Han, Yan Gao, Yao Hu, Shilin Zhang, and Hai Zhao. 2024. PyramidInfer: Pyramid KV Cache Compression for High-throughput LLM Inference. (2024). arXiv:cs.CL/2405.12532 <https://arxiv.org/abs/2405.12532>
- [49] Chaoran Zhang, Lixin Zou, Dan Luo, Min Tang, Xiangyang Luo, Zihao Li, and Chenliang Li. 2024. Efficient Sparse Attention needs Adaptive Token Release. (2024). arXiv:cs.CL/2407.02328 <https://arxiv.org/abs/2407.02328>
- [50] Lei Zhang, Yunshui Li, Jiaming Li, Xiaobo Xia, Jiayi Yang, Run Luo, Minzheng Wang, Longze Chen, Junhao Liu, and Min Yang. 2024. Hierarchical Context Pruning: Optimizing Real-World Code Completion with Repository-Level Pretrained Code LLMs. (2024). arXiv:cs.CL/2406.18294 <https://arxiv.org/abs/2406.18294>
- [51] Zhenyu Zhang, Ying Sheng, Tianyi Zhou, Tianlong Chen, Lianmin Zheng, Ruisi Cai, Zhao Song, Yuandong Tian, Christopher Ré, Clark Barrett, Zhangyang "Atlas" Wang, and Beidi Chen. 2023. H2O: Heavy-Hitter Oracle for Efficient Generative Inference of Large Language Models. In *Advances in Neural Information Processing Systems*, A. Oh, T. Neumann, A. Globerson, K. Saenko,

M. Hardt, and S. Levine (Eds.), Vol. 36. Curran Associates, Inc., 34661–34710. https://proceedings.neurips.cc/paper_files/paper/2023/file/6ceefa7b15572587b78ecfceb2827f8-Paper-Conference.pdf

[52] Yinmin Zhong, Shengyu Liu, Junda Chen, Jianbo Hu, Yibo Zhu, Xuanzhe Liu, Xin Jin, and Hao Zhang. 2024. DistServe: Disaggregating

Prefill and Decoding for Goodput-optimized Large Language Model Serving. In *18th USENIX Symposium on Operating Systems Design and Implementation (OSDI 24)*. USENIX Association, Santa Clara, CA, 193–210. <https://www.usenix.org/conference/osdi24/presentation/zhong-yinmin>